

Field induced Chern insulating states in twisted monolayer–bilayer graphene

Zhengwen Wang(王政文), Yingzhuo Han(韩英卓), Kenji Watanabe, Takashi Taniguchi, Yuhang Jiang(姜宇航), and Jinhai Mao(毛金海)

Citation: Chin. Phys. B, 2024, 33 (**6**): 067301. DOI: 10.1088/1674-1056/ad3b8a
Journal homepage: http://cpb.iphy.ac.cn; http://iopscience.iop.org/cpb

What follows is a list of articles you may be interested in

Light-modulated graphene-based φ_0 Josephson junction and $-\varphi_0$ to φ_0 transition

Renxiang Cheng(程任翔), Miao Yu(于苗), Hong Wang(汪洪), Deliang Cao(曹德亮), Xingao Li(李兴鳌), Fenghua Qi(戚凤华), and Xingfei Zhou(周兴飞)

Chin. Phys. B, 2024, 33 (**2**): 027302. DOI: 10.1088/1674-1056/ad04c5

Effects of strain on the flat band in twisted bilayer graphene

Zhen Zhang(张镇), Lu Wen(文露), Youkai Qiao(乔友凯), and Zhiqiang Li(李志强)

Chin. Phys. B, 2023, 32 (**10**): 107302. DOI: 10.1088/1674-1056/acb2c1

Recent advances of defect-induced spin and valley polarized states in graphene

Yu Zhang(张钰), Liangguang Jia(贾亮广), Yaoyao Chen(陈瑶瑶), Lin He(何林), and Yeliang Wang(王业亮)

Chin. Phys. B, 2022, 31 (**8**): 087301. DOI: 10.1088/1674-1056/ac70c4

Anisotropic refraction and valley-spin-dependent anomalous Klein tunneling in a 1T'-MoS_2-based p-n junction

Fenghua Qi(戚凤华) and Xingfei Zhou(周兴飞)

Chin. Phys. B, 2022, 31 (**7**): 077301. DOI: 10.1088/1674-1056/ac46bf

A facile and efficient dry transfer technique for two-dimensional Van der Waals heterostructure

Li Xie(谢立), Luojun Du(杜罗军), Xiaobo Lu(卢晓波), Rong Yang(杨蓉), Dongxia Shi(时东霞), Guangyu Zhang(张广宇)

Chin. Phys. B, 2017, 26 (**8**): 087306. DOI: 10.1088/1674-1056/26/8/087306

RAPID COMMUNICATION

Field induced Chern insulating states in twisted monolayer–bilayer graphene

Zhengwen Wang(王政文)[1,2], Yingzhuo Han(韩英卓)[1], Kenji Watanabe[3], Takashi Taniguchi[3], Yuhang Jiang(姜宇航)[2,†], and Jinhai Mao(毛金海)[1,‡]

[1] *School of Physical Science and CAS Center for Excellence in Topological Quantum Computation, University of Chinese Academy of Sciences, Beijing* 100049, *China*

[2] *College of Materials Science and Optoelectronic Technology, Center of Materials Science and Optoelectronics Engineering, University of Chinese Academy of Sciences, Beijing* 100049, *China*

[3] *Advanced Materials Laboratory, National Institute for Materials Science, Tsukuba* 305-0044, *Japan*

(Received 9 March 2024; revised manuscript received 7 April 2024; accepted manuscript online 7 April 2024)

Unraveling the mechanism underlying topological phases, notably the Chern insulators (ChIs) in strong correlated systems at the microscopy scale, has captivated significant research interest. Nonetheless, ChIs harboring topological information have not always manifested themselves, owing to the constraints imposed by displacement fields in certain experimental configurations. In this study, we employ density-tuned scanning tunneling microscopy (DT-STM) to investigate the ChIs in twisted monolayer–bilayer graphene (tMBG). At zero magnetic field, we observe correlated metallic states. While under a magnetic field, a metal–insulator transition happens and an integer ChI is formed emanating from the filling index $s = 3$ with a Chern number $C = 1$. Our results underscore the pivotal role of magnetic fields as a powerful probe for elucidating topological phases in twisted Van der Waals heterostructures.

Keywords: Chern insulators, strong correlation effects, two-dimensional van der Waals heterostructure, density-tuned scanning tunneling microscopy (DT-STM)

PACS: 73.22.Pr, 73.21.Cd, 68.37.Ef, 85.30.Tv **DOI:** 10.1088/1674-1056/ad3b8a

1. Introduction

Strong correlations among electrons in condensed matter systems give rise to a multitude of exotic emergent phenomena, including unconventional superconductivity,[1–6] heavy fermion behavior,[7–9] and correlated insulators (CIs).[10–12] CIs with non-trivial topological bands give rise to one of the most important research fields in condensed matter physics, Chern insulators (ChIs).[13–21] Unraveling the microscopic mechanisms underpinning these exotic states has become a topic of paramount importance in recent investigations. Scanning tunneling microscopy (STM), with unparalleled spatial and energy resolutions, offers a promising approach to exploring electronics structure on atomic scale. Combined STM with strongly correlated topological systems holds the potential to elucidate the intricate interplay between topological order, strong correlations, and material-specific details, paving the way for tailored engineering of novel topological phases.[22–25]

Twisted Van der Waals heterostructures with reconstructed moiré flat bands host strongly interacting electrons, where the Coulomb potential overwhelms the kinetic energy. These systems provide a highly tunable platform for exploring the rich landscape of strongly correlated physics.[26,27] A plethora of exotic correlation-driven electronic states have been observed and studied in various twisted van der Waals systems, including twisted bilayer graphene (TBG),[3,10,14,17,22,28–30] twisted double bilayer graphene (tDBG),[11,12,31–33] twisted monolayer–bilayer graphene (tMBG),[15,20,24,25,34–36] and twisted transition metal dichalcogenide (tTMD).[37–41] The tMBG system, consisting of a monolayer graphene stacked above Bernal-stacked bilayer graphene, provides an ideal platform for exploring the interplay between strong correlations and topological phases.[16,34] Transport studies have revealed abundant topological phases in tMBG,[15,20,34,35] direct microscopic evidence to construct a comprehensive understanding of the underlying mechanisms remains scarce, necessitating further local probe studies such as STM investigations.

Naturally, the realization of CIs is a prerequisite to explore ChIs in twisted Van der Waals heterostructures.[13,14,17] However, CIs are sensitive to the direction and strength of the displacement field, leading to the emergence of correlated metallic states instead of CIs under certain experimental parameters.[15,34] When faced with such situations, it becomes essential to implement strategies to induce CIs for the study of ChIs.

In this study, we employ a magnetic field to induce CIs in tMBG and identify its topological nature as an integer ChI.

[†]Corresponding author. E-mail: yuhangjiang@ucas.ac.cn

[‡]Corresponding author. E-mail: jhmao@ucas.ac.cn

© 2024 Chinese Physical Society and IOP Publishing Ltd

At zero magnetic field, the system exhibits a correlated metallic state, characterized by a flat band peak pinned at the Fermi level. While under high magnetic fields, the system undergoes a metal–insulator transition, exhibiting a CI near integer filling factors. We derive its topological quantum number (Chern number C, band filling index s) to be (1, 3), thereby confirming its nature as an integer Chern insulator. Our findings demonstrate that magnetic fields serve as a powerful tuning knob to explore correlation effects in two-dimensional materials.

2. Band structure of tMBG

Figure 1(a) illustrates the STM experimental setup and schematic structure of the tMBG device employed in this work. We construct our tMBG device by stacking a monolayer graphene atop a bilayer graphene (see SI for more details). The topography and electronic structure information can be probed by the STM tip, providing direct access to the correlated states of interest. The heavily hole-doped silicon substrate serves as a global gate, allowing for continuous tuning of the carrier density in the tMBG system by adjusting the back-gate voltage. Figure 1(b) shows a moiré superlattice with a period of 12.1 nm. The twist angle can be deduced to be $\theta = 1.17^\circ$ from the equation $L = a/(2\sin(\theta/2))$, where L is the moiré superlattice period, a is the crystal constant of graphene and θ is the twist angle. The black dashed lines and circles outline the moiré unit cell of the superlattice. Three high-symmetry regions with distinct local stacking orders are marked as 'ABB', 'ABC', and 'ABA' in Fig. 1(b). Similar to twisted bilayer graphene (TBG), the low-energy electronic structure of tMBG is characterized by two flat bands near the Fermi level. Figure 1(c) demonstrates the calculated low energy band structure of the tMBG system with $\theta = 1.17^\circ$ using the continuous model (see SI for more details). The two red bands are the conduction flat band (CFB) and the valence flat band (VFB), respectively. Each flat band holds a four-fold degeneracy due to the spin and valley degrees of freedom. Figure 1(d) presents $\mathrm{d}I/\mathrm{d}V$ spectra taken at the ABB region with filling factor $\nu = +4$, which ensures the complete filling of the flat bands with electrons. The relationship between filling factor ν and back-gate voltage V_g can be described with the equation $\nu = 8 \cdot \frac{(V_\mathrm{g} - V_\mathrm{CNP})}{V_\mathrm{F} - V_\mathrm{E}}$, where $V_\mathrm{CNP} = (V_\mathrm{F} + V_\mathrm{E})/2$ is the back-gate corresponding to the charge neutral point, V_F and V_E are the back gates corresponding to full and empty filling of the flat band with electrons, which can be determined from the gate-dependent $\mathrm{d}I/\mathrm{d}V$ spectra (see SI for more details). The $\mathrm{d}I/\mathrm{d}V$ spectra in ABA and ABC regions are similar with those in ABB region (see SI). All the subsequent spectra were taken at the ABB region unless otherwise specified. Below the Fermi level, two prominent features corresponding to the CFB and VFB are observed, consistent with the band structure calculations.

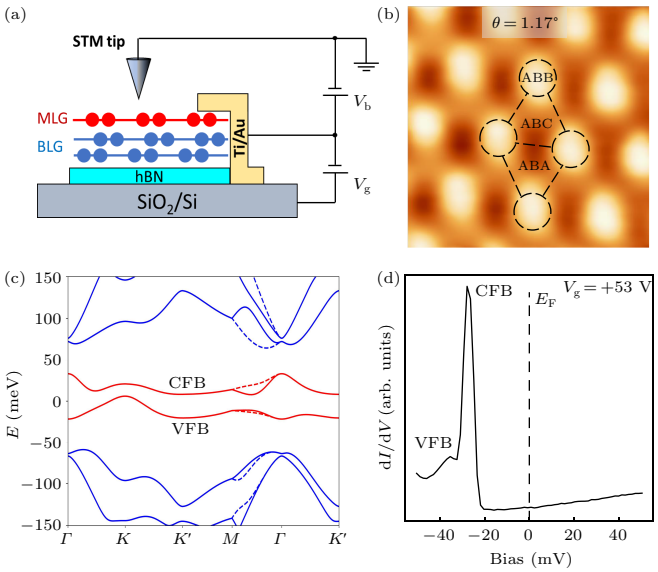


Fig. 1. (a) The sketch of our experiment setup, the electronic structure was detected from the monolayer side of tMBG. The carrier density was tuned by the back-gate voltage V_g from the doped Si substrate. (b) The topography of the moiré superlattice with twist angle $\theta = 1.17^\circ$, three high symmetry regions represented by 'ABB', 'ABC', 'ABA' in the moiré unit cell were depicted ($V_\mathrm{b} = -150$ mV, $I = 80$ pA). (c) The band structure of tMBG with twisted angle $\theta = 1.17^\circ$ calculated by continuous model. Two flat bands in red color near the Fermi level are marked as 'CFB' and 'VFB'. (d) $\mathrm{d}I/\mathrm{d}V$ spectra at $V_\mathrm{g} = +53$ V (fully filling the flat band). The CFB and VFB were characterized by two peaks below the Fermi level ($V_\mathrm{b} = -150$ mV, $I = 80$ pA, $V_\mathrm{m} = 3$ mV).

3. Metal–insulating transition under magnetic field

To investigate correlation effects in this flat band system, it is crucial to tune the carrier density to partially fill the flat bands, thereby maximizing the electron–electron interactions. Figure 2(a) first shows gate-dependent $\mathrm{d}I/\mathrm{d}V$ spectra at zero magnetic field. The $\mathrm{d}I/\mathrm{d}V$ spectra consistently exhibit a finite intensity at the Fermi level without any gap feature formed as the carrier density is continuously tuned. This behavior suggests that at $B = 0$ T, the tMBG system resides in the correlated metallic state regime, characterized by the conduction flat band pinned at the Fermi level (see SI for more details). Figure 2(b) presents the spectra series within the white dashed box in Fig. 2(a) from $V_\mathrm{g} = 33.0$ V ($\nu = 2.7$) to $V_\mathrm{g} = 44.0$ V ($\nu = 3.6$), clearly revealing a peak pinned at the Fermi level.

While subjected to a magnetic field of 4.0 T, as shown in Fig. 2(c), a metal–insulator transition with a gap opening is observed. The insulating gap emerges and persists over a wide doping range from $V_\mathrm{g} = 34.0$ V ($\nu = 2.7$) to fully filling the flat band. Interestingly, the insulating gap size evolves with the gate voltage, as depicted by the white dashed box in Fig. 2(c). Initially, the gap widens as the gate voltage increases, reaches a maximum, and then shrinks upon further gating. The maximized gap, indicated by the red arrow in Fig. 2(c), is identified as the CI.[25] To visualize this process more clearly, figure 2(d) plots the $\mathrm{d}I/\mathrm{d}V$ spectra within the white dashed box in Fig. 2(c). The size of the gap follows a

pattern of initial increase and subsequent decrease along with doping, as illustrated in Fig. 2(e). The red spectra line represents the maximum gap state at a gate voltage $V_g = 39.0$ V ($\nu = 3.2$).

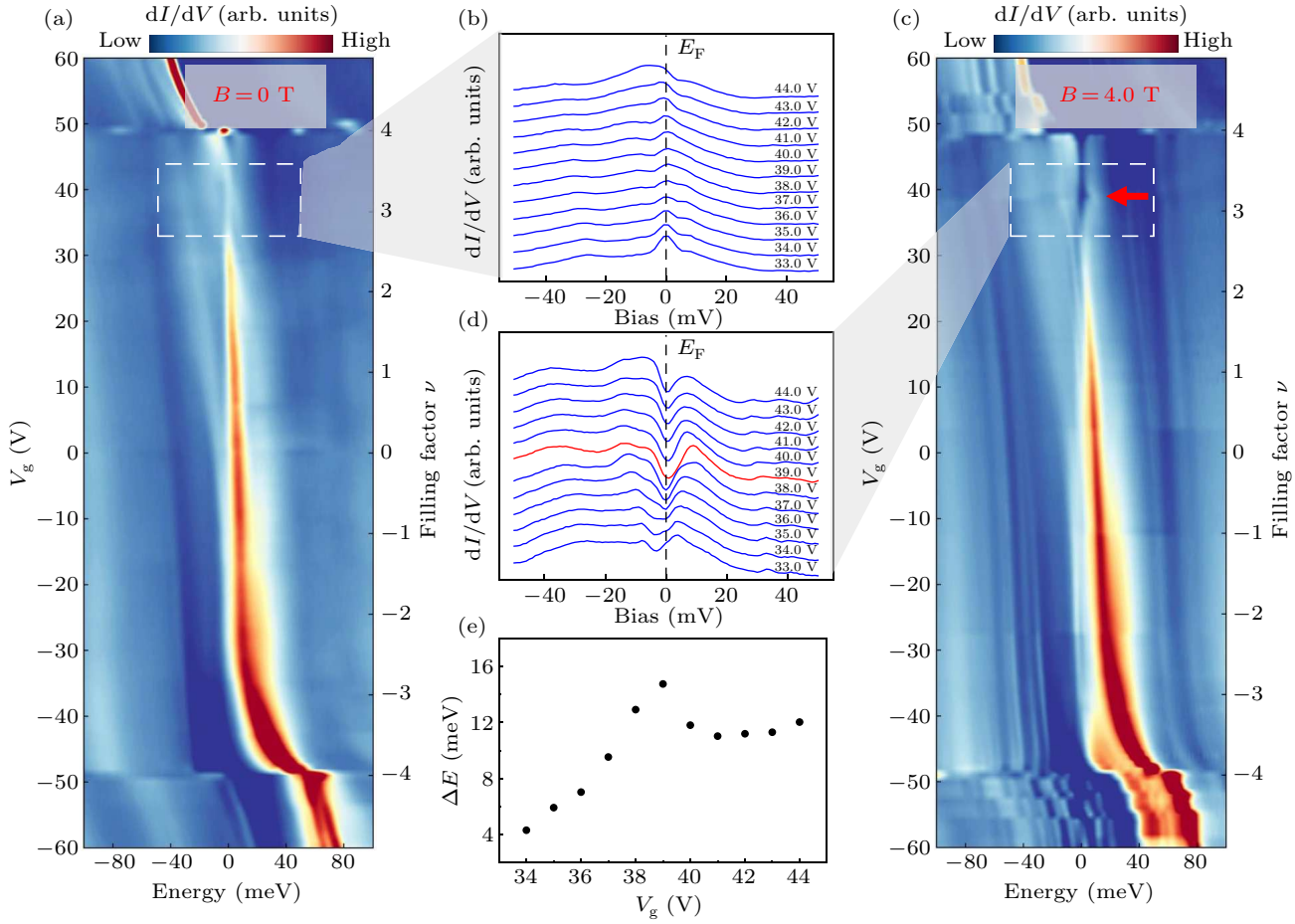


Fig. 2. (a), (b) Gate-dependent $\mathrm{d}I/\mathrm{d}V$ spectra at $B = 0$ T, the white dashed box indicates the selected area around filling factor $\nu = 3$ which is presented in a waterfall plot in (b) ($V_b = -150$ mV, $I = 80$ pA, $V_m = 3$ mV). (c) Gate-dependent $\mathrm{d}I/\mathrm{d}V$ spectra at $B = 4.0$ T, the red arrow highlights the correlated insulating state ($V_b = -100$ mV, $I = 500$ pA, $V_m = 1$ mV). (d) The waterfall plot of the spectra within the white dashed box region in panel (c). The spectra in red line represent the correlated insulating state. (e) The scatter plot of the gap size (ΔE) of the spectra in panel (d) as a function of gate voltage V_g.

4. Integer Chern insulating state

To elucidate the topological properties of the correlated insulating state, magnetic field-dependent $\mathrm{d}I/\mathrm{d}V$ spectra were acquired to track the Chern numbers of the gapped state.[14] Precisely, the topological property of a gapped state in a two-dimensional system can be characterized by quantum numbers (C, s) with the Diophantine equation $\nu = C\phi/\phi_0 + s$,[42] where ν is the filling factor of the CI at finite magnetic field, ϕ/ϕ_0 is the number of magnetic flux quanta of each moiré unit cell, C is the Chern number and s is the corresponding band filling index of the gapped state emanated from zero field. When the Chern number $C \neq 0$, the system is topologically non-trivial, the filling factor of the corresponding gap state evolves linearly with the magnetic field. Following this principle, we measured gate-dependent $\mathrm{d}I/\mathrm{d}V$ spectra at different magnetic fields. In Figs. 3(a)–3(e) we present zoomed-in gate-dependent $\mathrm{d}I/\mathrm{d}V$ spectra from $B = 2.0$ T to $B = 10.0$ T to show the evolution of the CI with the varied magnetic field. The CI in each magnetic field is identified and indicated by red arrows. The CI systematically shifts and its gap grows with increasing magnetic field strength. Figure 3(f) gathers $\mathrm{d}I/\mathrm{d}V$ spectra of the identified CI at varied magnetic fields. Gap states within the CI are indicated by red arrows. The evolution of the gap size as a function of the magnetic field is depicted in Fig. 3(g), revealing a monotonic increase in the gap size with increasing magnetic field strength. To determine the evolution of the CI with the magnetic field, we fitted our data to the Diophantine equation, as shown in Fig. 3(h). The error bars of the data represent the gate uncertainty of the identified CI, determined by the gate interval between two adjacent $\mathrm{d}I/\mathrm{d}V$ spectra of the gate-dependent $\mathrm{d}I/\mathrm{d}V$ spectra. The linear fitting result is shown by the red shade line, yielding the topological quantum numbers ($C = 1$, $s = 3$) (see SI for more details). The integer value of Chern number rules out the single particle band gap and trivial charge order state.[41,43] The band filling index is also an integer, which eliminates the fractional nature.[42] These findings identify that this gap state is an integer ChI.[14]

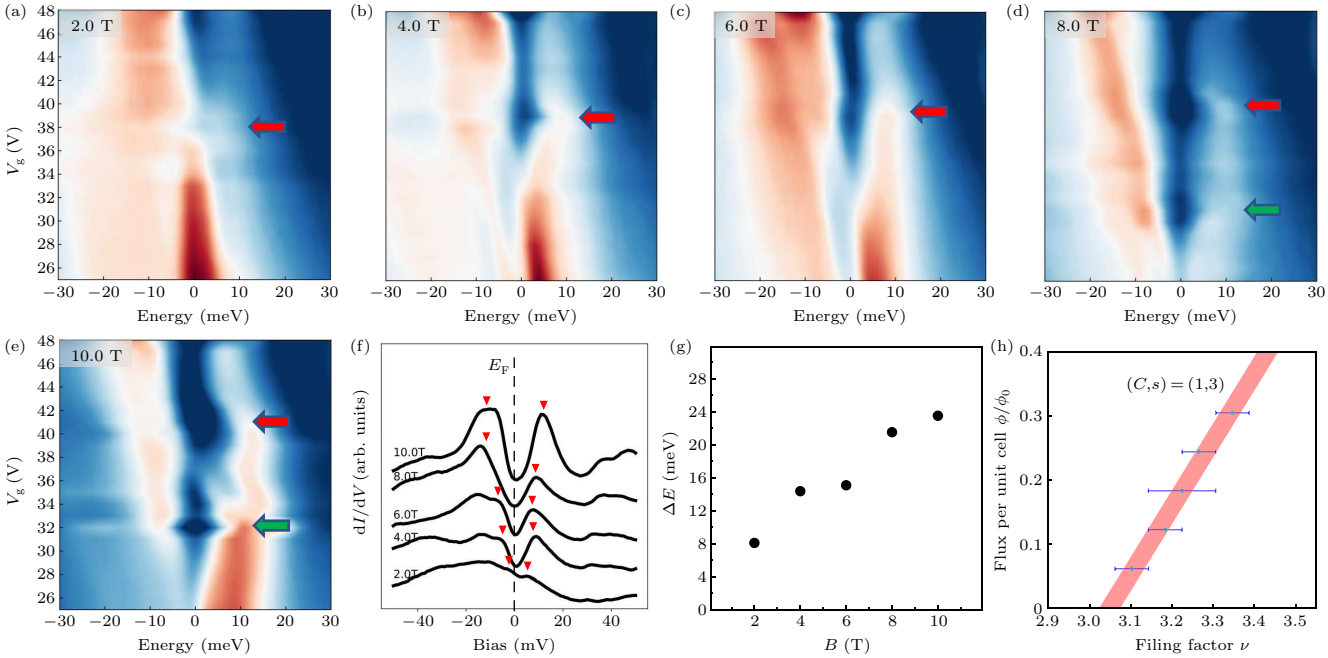


Fig. 3. (a)–(e) Zoomed-in gate-dependent dI/dV spectra around the correlated insulating state area from $B = 2.0$ T to $B = 10.0$ T. The red and green arrows indicate the correlated insulating states at each magnetic field ($V_b = -100$ mV, $I = 500$ pA, $V_m = 1$ mV). (f) Collection of correlated insulating states at different magnetic fields. The red arrows indicate the gap edges. (g) The scatter plot of the gap size (ΔE) of the spectra in panel (f) as a function of magnetic field (B). (h) The number of magnetic flux quanta per superlattice unit cell ϕ/ϕ_0 plotted versus flat band filling factor ν of CIs at different fields. The red line shows the linear fit to the data, giving the (C, s) of this ChI to be $(1, 3)$.

Furthermore, when the magnetic field exceeds 6.0 T, a new correlated insulating state emerges, as indicated by the green arrows in Figs. 3(d) and 3(e), which further substantiate the potency of the magnetic field.

5. Conclusion and perspectives

In conclusion, we use DT-STM to investigate correlation effects in tMBG. At zero magnetic field, a correlated metallic state is observed and characterized by the flat band pinned to the Fermi level. While subjected to high magnetic field, a metal–insulator transition occurs, and CI emerges, identified as the maximized gap states in the gate-dependent dI/dV spectra. Moreover, the filling factor of the CI evolves linearly with varying magnetic fields, suggesting that this CI is topological non-trivial. We extract the topological quantum numbers of the CI to be $(C = 1, s = 3)$ which classifies this CI as an integer ChI. Our results demonstrate the utility of magnetic fields as a powerful tool to induce CI and unveil the hidden topological phase in tMBG. This strategy emphasizes the crucial role played by magnetic fields in exploring correlation effects in twisted van der Waals heterostructures.

Acknowledgements

Project supported by the National Natural Science Foundation of China (Grant No. 12074377 (Y.J.)), Fundamental Research Funds for the Central Universities (J.M. and Y.J.), the International Partnership Program of Chinese Academy of Sciences (Grant No. 211211KYSB20210007), and the Beijing Outstanding Young Scientist Program.

References

[1] Bok J M, Bae J J, Choi H Y, Varma C M, Zhang W, He J, Zhang Y, Yu L and Zhou X J 2016 *Sci. Adv.* **2** e1501329
[2] Garg A, Randeria M and Trivedi N 2008 *Nat. Phys.* **4** 762
[3] Cao Y, Fatemi V, Fang S, Watanabe K, Taniguchi T, Kaxiras E and Jarillo-Herrero P 2018 *Nature* **556** 43
[4] Lake E and Senthil T 2021 *Phys. Rev. B* **104** 174505
[5] Oh M, Nuckolls K P, Wong D, Lee R L, Liu X, Watanabe K, Taniguchi T and Yazdani A 2021 *Nature* **600** 240
[6] Kim H, Choi Y, Lewandowski C, Thomson A, Zhang Y, Polski R, Watanabe K, Taniguchi T, Alicea J and Nadj-Perge S 2022 *Nature* **606** 494
[7] Arita R, Held K, Lukoyanov A V and Anisimov V I 2007 *Phys. Rev. Lett.* **98** 166402
[8] Gegenwart P, Si Q and Steglich F 2008 *Nat. Phys.* **4** 186
[9] Aynajian P, da Silva Neto E H, Gyenis A, Baumbach R E, Thompson J D, Fisk Z, Bauer E D and Yazdani A 2012 *Nature* **486** 201
[10] Cao Y, Fatemi V, Demir A, Fang S, Tomarken S L, Luo J Y, Sanchez-Yamagishi J D, Watanabe K, Taniguchi T, Kaxiras E, Ashoori R C and Jarillo-Herrero P 2018 *Nature* **556** 80
[11] Cao Y, Rodan-Legrain D, Rubies-Bigorda O, Park J M, Watanabe K, Taniguchi T and Jarillo-Herrero P 2020 *Nature* **583** 215
[12] Shen C, Chu Y, Wu Q, Li N, Wang S, Zhao Y, Tang J, Liu J, Tian J, Watanabe K, Taniguchi T, Yang R, Meng Z Y, Shi D, Yazyev O V and Zhang G 2020 *Nat. Phys.* **16** 520
[13] Chen G, Sharpe A L, Fox E J, Zhang Y H, Wang S, Jiang L, Lyu B, Li H, Watanabe K, Taniguchi T, Shi Z, Senthil T, Goldhaber-Gordon D, Zhang Y and Wang F 2020 *Nature* **579** 56
[14] Nuckolls K P, Oh M, Wong D, Lian B, Watanabe K, Taniguchi T, Bernevig B A and Yazdani A 2020 *Nature* **588** 610
[15] Polshyn H, Zhu J, Kumar M A, Zhang Y, Yang F, Tschirhart C L, Serlin M, Watanabe K, Taniguchi T, MacDonald A H and Young A F 2020 *Nature* **588** 66
[16] Rademaker L, Protopopov I V and Abanin D A 2020 *Phys. Rev. Res.* **2** 033150
[17] Choi Y, Kim H, Peng Y, Thomson A, Lewandowski C, Polski R, Zhang Y, Arora H S, Watanabe K, Taniguchi T, Alicea J and Nadj-Perge S 2021 *Nature* **589** 536

[18] Pierce A T, Xie Y, Park J M, Khalaf E, Lee S H, Cao Y, Parker D E, Forrester P R, Chen S, Watanabe K, Taniguchi T, Vishwanath A, Jarillo-Herrero P and Yacoby A 2021 *Nat. Phys.* **17** 1210

[19] Grover S, Bocarsly M, Uri A, Stepanov P, Di Battista G, Roy I, Xiao J, Meltzer A Y, Myasoedov Y, Pareek K, Watanabe K, Taniguchi T, Yan B, Stern A, Berg E, Efetov D K and Zeldov E 2022 *Nat. Phys.* **18** 885

[20] Polshyn H, Zhang Y, Kumar M A, Soejima T, Ledwith P, Watanabe K, Taniguchi T, Vishwanath A, Zaletel M P and Young A F 2022 *Nat. Phys.* **18** 42

[21] Yu J, Foutty B A, Han Z, Barber M E, Schattner Y, Watanabe K, Taniguchi T, Phillips P, Shen Z X, Kivelson S A and Feldman B E 2022 *Nat. Phys.* **18** 825

[22] Jiang Y, Lai X, Watanabe K, Taniguchi T, Haule K, Mao J and Andrei E Y 2019 *Nature* **573** 91

[23] Wong D, Nuckolls K P, Oh M, Lian B, Xie Y, Jeon S, Watanabe K, Taniguchi T, Bernevig B A and Yazdani A 2020 *Nature* **582** 198

[24] Li S Y, Wang Z, Xue Y, Wang Y, Zhang S, Liu J, Zhu Z, Watanabe K, Taniguchi T, Gao H J, Jiang Y and Mao J 2022 *Nat. Commun.* **13** 4225

[25] Zhang C, Zhu T, Soejima T, Kahn S, Watanabe K, Taniguchi T, Zettl A, Wang F, Zaletel M P and Crommie M F 2023 *Nat. Commun.* **14** 3595

[26] Yankowitz M, Ma Q, Jarillo-Herrero P and LeRoy B J 2019 *Nat. Rev. Phys.* **1** 112

[27] Behura S K, Miranda A, Nayak S, Johnson K, Das P and Pradhan N R 2021 *Emergent Mater.* **4** 813

[28] Xie Y, Pierce A T, Park J M, Parker D E, Khalaf E, Ledwith P, Cao Y, Lee S H, Chen S, Forrester P R, Watanabe K, Taniguchi T, Vishwanath A, Jarillo-Herrero P and Yacoby A 2021 *Nature* **600** 439

[29] Bhowmik S, Ghawri B, Leconte N, Appalakondaiah S, Pandey M, Mahapatra P S, Lee D, Watanabe K, Taniguchi T, Jung J, Ghosh A and Chandni U 2022 *Nat. Phys.* **18** 639

[30] Li X F, Sun R X, Wang S Y, Li X, Liu Z B and Tian J G 2022 *Chin. Phys. Lett.* **39** 037301

[31] He M, Li Y, Cai J, Liu Y, Watanabe K, Taniguchi T, Xu X and Yankowitz M 2021 *Nat. Phys.* **17** 26

[32] Liu X, Chiu C L, Lee J Y, Farahi G, Watanabe K, Taniguchi T, Vishwanath A and Yazdani A 2021 *Nat. Commun.* **12** 2732

[33] Rubio-Verdú C, Turkel S, Song Y, Klebl L, Samajdar R, Scheurer M S, Venderbos J W F, Watanabe K, Taniguchi T, Ochoa H, Xian L, Kennes D M, Fernandes R M, Rubio Á and Pasupathy A N 2022 *Nat. Phys.* **18** 196

[34] Chen S, He M, Zhang Y H, Hsieh V, Fei Z, Watanabe K, Taniguchi T, Cobden D H, Xu X, Dean C R and Yankowitz M 2021 *Nat. Phys.* **17** 374

[35] Xu S, Al Ezzi M M, Balakrishnan N, Garcia-Ruiz A, Tsim B, Mullan C, Barrier J, Xin N, Piot B A, Taniguchi T, Watanabe K, Carvalho A, Mishchenko A, Geim A K, Fal'ko V I, Adam S, Neto A H C, Novoselov K S and Shi Y 2021 *Nat. Phys.* **17** 619

[36] Li S, Wang Z, Xue Y, Cao L, Watanabe K, Taniguchi T, Gao H and Mao J 2023 *Chin. Phys. B* **32** 067304

[37] Tong Q, Yu H, Zhu Q, Wang Y, Xu X and Yao W 2017 *Nat. Phys.* **13** 356

[38] Tran K, Moody G, Wu F, *et al.* 2019 *Nature* **567** 71

[39] Xu Y, Liu S, Rhodes D A, Watanabe K, Taniguchi T, Hone J, Elser V, Mak K F and Shan J 2020 *Nature* **587** 214

[40] Huang X, Wang T, Miao S, Wang C, Li Z, Lian Z, Taniguchi T, Watanabe K, Okamoto S, Xiao D, Shi S F and Cui Y T 2021 *Nat. Phys.* **17** 715

[41] Kometter C R, Yu J, Devakul T, Reddy A P, Zhang Y, Foutty B A, Watanabe K, Taniguchi T, Fu L and Feldman B E 2023 *Nat. Phys.* **19** 1861

[42] Spanton E M, Zibrov A A, Zhou H, Taniguchi T, Watanabe K, Zaletel M P and Young A F 2018 *Science* **360** 62

[43] Cao Y, Luo J Y, Fatemi V, Fang S, Sanchez-Yamagishi J D, Watanabe K, Taniguchi T, Kaxiras E and Jarillo-Herrero P 2016 *Phys. Rev. Lett.* **117** 116804